Bmi1 overexpression in the cerebellar granule cell lineage of mice affects cell proliferation and survival without initiating medulloblastoma formation

Hourinaz Behesti[1,*], Heeta Bhagat[1], Adrian M. Dubuc[2,3,4], Michael D. Taylor[2,3,4] and Silvia Marino[1,‡]

SUMMARY

BMI1 is a potent inducer of neural stem cell self-renewal and neural progenitor cell proliferation during development and in adult tissue homeostasis. It is overexpressed in numerous human cancers – including medulloblastomas, in which its functional role is unclear. We generated transgenic mouse lines with targeted overexpression of *Bmi1* in the cerebellar granule cell lineage, a cell type that has been shown to act as a cell of origin for medulloblastomas. Overexpression of *Bmi1* in granule cell progenitors (GCPs) led to a decrease in cerebellar size due to decreased GCP proliferation and repression of the expression of cyclin genes, whereas *Bmi1* overexpression in postmitotic granule cells improved cell survival in response to stress by altering the expression of genes in the mitochondrial cell death pathway and of *Myc* and *Lef-1*. Although no medulloblastomas developed in ageing cohorts of transgenic mice, crosses with *Trp53*^{−/−} mice resulted in a low incidence of medulloblastoma formation. Furthermore, analysis of a large collection of primary human medulloblastomas revealed that tumours with a *BMI1*^{high} *TP53*^{low} molecular profile are significantly enriched in Group 4 human medulloblastomas. Our data suggest that different levels and timing of *Bmi1* overexpression yield distinct cellular outcomes within the same cellular lineage. Importantly, *Bmi1* overexpression at the GCP stage does not induce tumour formation, suggesting that *BMI1* overexpression in GCP-derived human medulloblastomas probably occurs during later stages of oncogenesis and might serve to enhance tumour cell survival.

INTRODUCTION

Medulloblastoma is a malignant paediatric cerebellar tumour that can arise from cerebellar granule cell progenitors (GCPs), as shown by conditional mouse models with compound homozygous mutations in *Rb* and *Trp53* (Marino et al., 2000) or heterozygosity in patched1 (*Ptch1*) (Schuller et al., 2008; Yang et al., 2008). Cerebellar granule cells, the most populous neuronal cell type of the mammalian central nervous system (CNS), originate from the upper rhombic lip upon expression of *Math1* (atonal homologue 1), amongst other genes (Machold and Fishell, 2005; Wingate and Hatten, 1999). Upon specification, they migrate to form the external granule cell layer (EGL), where they proliferate extensively for up to 3 weeks, including the first two postnatal weeks in the mouse (Behesti and Marino, 2009). Their differentiation is marked by the

downregulation of *Math1* expression and upregulation of mature granule cell markers such as γ-aminobutyric acid type A receptor α6 (GABRA6) (Kato, 1990; Mullen et al., 1992).

BMI1 is an epigenetic gene repressor (Valk-Lingbeek et al., 2004) expressed at high levels in human and mouse proliferating GCPs, and at low levels in postmitotic granule cells. Moreover, it is overexpressed in several human cancers, including medulloblastoma (Leung et al., 2004). The role of *BMI1* overexpression in medulloblastoma pathogenesis is currently not clear. *Bmi1*^{−/−} mice display reduced GCP proliferation (Leung et al., 2004; van der Lugt et al., 1994) and reduced subventricular zone neural stem cell (NSC) self-renewal (Molofsky et al., 2003), indicating a role for *Bmi1* in normal stem and progenitor cell proliferation. Although BMI1 acts in a multimeric protein complex, it induces lymphoma formation when overexpressed alone in the lymphoid compartment (Haupt et al., 1993). In the mouse CNS, *Bmi1* overexpression driven by the nestin promoter was shown to increase NSC self-renewal in vitro but not in vivo (He et al., 2009), whereas lentiviral overexpression in the embryonic and adult cortices as well as conditional overexpression in nestin-positive radial glial cells and progenitors derived thereof resulted in increased cell proliferation both in vitro and in vivo (Fasano et al., 2009; Yadirgi et al., 2011). The different experimental approaches and targeting of mixed populations of cells at different stages could account for the different observations in these studies. Clearly defined spatiotemporal overexpression of *Bmi1* in a known cell of origin of a CNS tumour is therefore required to understand the role of BMI1 overexpression in brain oncogenesis.

In cancer cells, deregulation of several processes, apart from cell proliferation, have been described, including resistance to apoptosis and the ability to withstand a higher metabolic rate, which requires

[1]Blizard Institute of Cell and Molecular Science, Barts and the London School of Medicine and Dentistry, Queen Mary University of London, 4 Newark Street, London, E1 2AT, UK
[2]Division of Neurosurgery, Arthur and Sonia Labatt Brain Tumour Research Centre, The Hospital for Sick Children, Toronto, Ontario, Canada
[3]Program in Developmental and Stem Cell Biology, The Hospital for Sick Children, Toronto, Ontario, Canada
[4]Department of Laboratory Medicine and Pathobiology, University of Toronto, Toronto, Ontario, Canada
*Present address: Rockefeller University, Laboratory of Developmental Neurobiology, 1230 York Avenue, New York, NY 10065, USA
‡Author for correspondence (s.marino@qmul.ac.uk)

Disease Models & Mechanisms • DMM

TRANSLATIONAL IMPACT

Clinical issue
BMI1 is an epigenetic gene regulator that has gained considerable interest in the field of stem cell biology because it is a potent inducer of neural stem cell self-renewal in vitro and in vivo. The ability of BMI1 to induce stem cell self-renewal might be beneficial in regenerative medicine, but its abnormally high expression levels in various cancers raises the issue of whether BMI1 can initiate tumours or contribute to tumourigenesis if overexpressed in the wrong cell at the wrong time. The aim of this study was to examine the effect of BMI1 overexpression in the granule cell lineage (a cell type that can be the origin of medulloblastomas) in the context of medulloblastoma formation and the control of cellular processes linked to oncogenesis.

Results
The authors generated and examined transgenic mice overexpressing BMI1 specifically in the granule cell lineage. Their findings suggest that BMI1 does not initiate tumorigenesis on its own, but that its overexpression affects distinct cellular processes and molecular pathways depending on the ontogeny of the cell at the time of overexpression. It improves the survival of postmitotic granule cells under stress, while decreasing the proliferation of granule cell progenitors. However, a low incidence of medulloblastoma was detected when BMI1 overexpression was induced in a $Trp53^{-/-}$ background. Human medulloblastoma is classified into four groups according to gene expression profiles; here, the authors found that human tumours with a $BMI1^{high}$ $TP53^{low}$ profile are significantly enriched in Group 4 human medulloblastomas.

Implications and future directions
These results indicate that BMI1 overexpression is not sufficient to induce neoplastic transformation and that it can induce medulloblastoma in mice only together with loss of p53, potentially mimicking human Group 4 medulloblastoma. These data also highlight a role for BMI1 overexpression in neuronal survival under stress conditions, a discovery that provides clues for future potential therapies related to regeneration and repair.

cancer cells to be superior at eliminating and/or better at tolerating toxins such as reactive oxygen species (ROS) produced by increased metabolism. ROS levels are higher than normal in several tissues in $Bmi1^{-/-}$ mice, owing to mitochondrial malfunction, resulting in activation of the DNA-damage response (DDR) pathway (Chatoo et al., 2009; Liu et al., 2009). It is therefore possible that $Bmi1$ overexpression serves as an antioxidant and pro-survival factor in medulloblastoma pathogenesis.

Here we investigated the effect of $Bmi1$ overexpression, specifically in the granule cell lineage, in medulloblastoma initiation and progression, and examined cell proliferation, differentiation and antioxidant defence mechanisms in transgenic mice and in the DAOY medulloblastoma cell line. Contrary to expectations, we detected a reduction in cerebellar size owing to decreased GCP proliferation, downregulation of positive regulators of the cell cycle and the downregulation of the DDR pathway upon $Bmi1$ overexpression in GCPs. $Bmi1$ overexpression in postmitotic cerebellar granule cells resulted in increased cell survival and changes in the mitochondrial cell death pathway and survival genes but not antioxidant genes. This suggests that $Bmi1$ overexpression can affect distinct cellular processes depending on the ontogenic stage of the cell in which it is overexpressed. No tumours were observed when $Bmi1$ was overexpressed in either proliferating progenitor or postmitotic granule cells, whereas crosses with tumour-prone $Trp53^{-/-}$ mice resulted in a low incidence of medulloblastoma formation. Moreover, gene profiling analysis

of a large human medulloblastoma dataset revealed enrichment of a $BMI1^{high}$ $TP53^{low}$ molecular signature in Group 4 medulloblastomas.

RESULTS

Overexpression of *Bmi1* in the granule cell lineage
To target $Bmi1$ overexpression to GCPs, the full-length $Bmi1$ cDNA was positioned downstream of a 1.4 kb enhancer sequence, found 3′ of the $Math1$ coding region (Fig. 1A). This regulatory sequence has previously been shown to drive GFP expression in GCPs but not in postmitotic granule cells in the developing cerebellum (Lumpkin et al., 2003). Four $Math1$-$Bmi1$ founder lines were generated, out of which two (named T25 and T26) exhibited a 1.5- to 2-fold increase in $Bmi1$ expression in comparison with wild-type levels in littermate controls, as assessed by quantitative reverse-transcription PCR (qRT-PCR) on RNA isolated from postnatal day 6 (P6) cerebella (Fig. 1B). These two lines were selected for further analysis. Immunohistochemical labelling of BMI1 in P6 cerebella confirmed increased expression of the protein in $Math1$-$Bmi1$ mice in the outer layer of the EGL, where proliferating GCPs are found (Fig. 1C).

To overexpress $Bmi1$ in postmitotic and mature cerebellar granule cells, the full-length $Bmi1$ cDNA was driven by a 6 kb fragment of the $Gabra6$ subunit gene (Fig. 1D). This sequence has previously been shown to drive gene expression in postmitotic (not progenitor) cerebellar granule cells from P8 onwards (Bahn et al., 1997). Two out of four $Gabra6$-$Bmi1$ transgenic founder lines (named T3 and T4) were selected for further analysis on the basis of increased $Bmi1$ gene expression levels quantified by qRT-PCR. Whereas a modest two-fold increase in $Bmi1$ expression was detected in transgenic cerebella at P9 (Fig. 1E), at 1 day after the reported onset of gene expression driven by the $Gabra6$ gene fragment, adult transgenic animals displayed on average a 14- to 15-fold increase in expression in comparison with wild-type littermates (Fig. 1E). Immunohistochemical labelling of P9 cerebella showed expression of BMI1 in the internal granule cell layer (IGL) of $Gabra6$-$Bmi1$ but not of wild-type cerebella (Fig. 1F). BMI1 protein expression detected by western blot of whole cerebella confirmed high levels of BMI1 expression in transgenic cerebella at P15, when endogenous levels are downregulated in wild-type littermates (Fig. 1H). The average level of $Bmi1$ overexpression detected in our transgenic mice ranged from 1.5- to 15-fold of normal $Bmi1$ expression in the cerebellum (Fig. 1B,E). To gain an indication of $BMI1$ expression levels in human medulloblastomas, qRT-PCR was performed on six primary tumour samples and results compared with those for normal human fetal cerebella. $BMI1$ expression in human medulloblastoma samples was found to be 2- to 14-fold higher than levels in normal cerebellar tissue (average 9±4 s.d., n=6 medulloblastomas; Fig. 1G). The expression levels detected in the transgenic mouse lines were therefore in line with the range observed in human medulloblastomas. All findings presented here were verified in two independently generated transgenic lines for each construct.

Histological and immunohistochemical analyses of cerebella at P6 in $Math1$-$Bmi1$ mice and at P30 in $Gabra6$-$Bmi1$ mice revealed that the overall cerebellar cytoarchitecture was normal and that all cell types (neurons, macroglia and microglia) were present in the transgenic animals (data not shown).
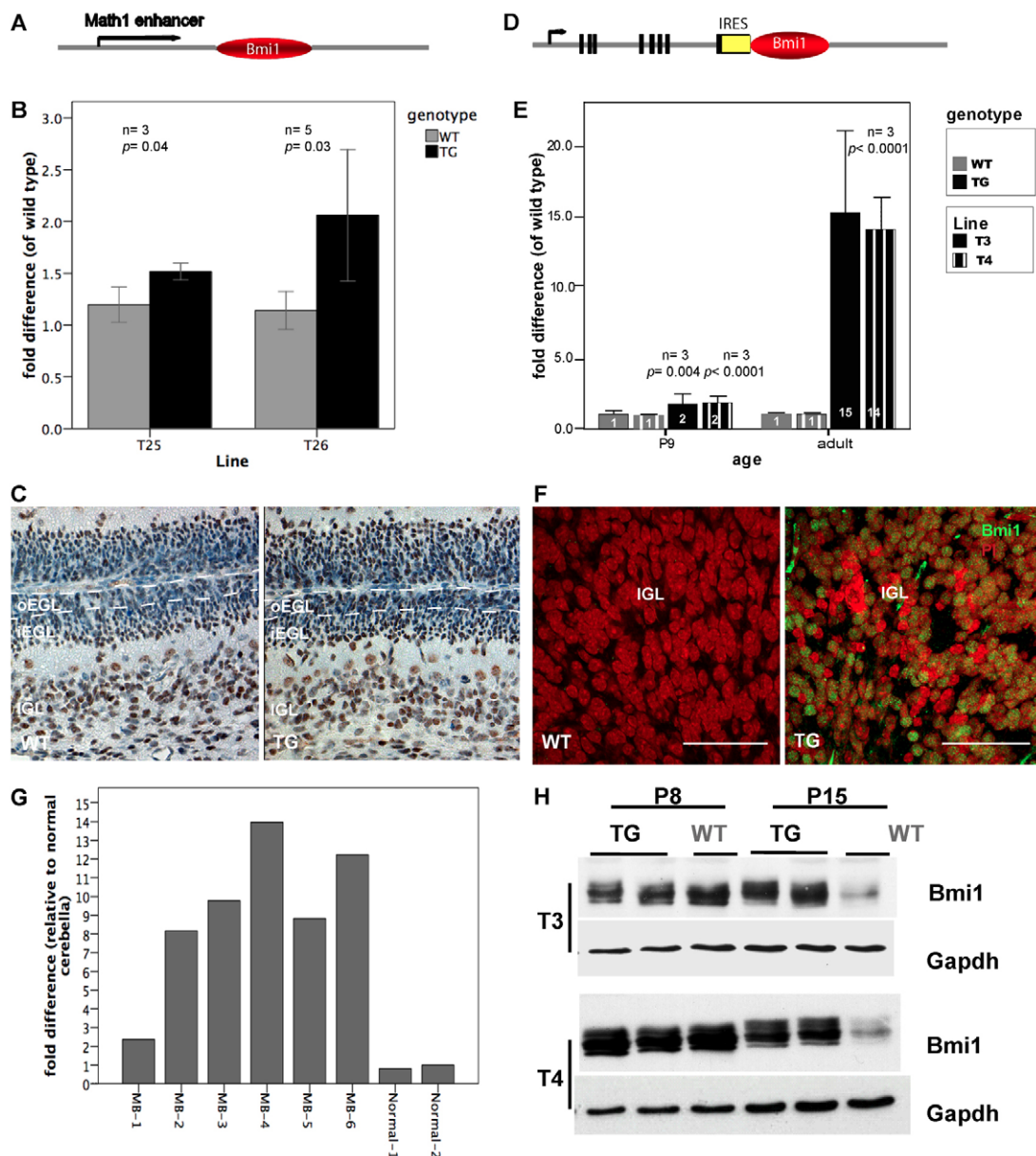
Fig. 1. BMI1 expression in human medulloblastomas and transgenic mouse lines. (A) Schematic of the *Math1-Bmi1* construct. (B) Fold increase in *Bmi1* expression in two *Math1-Bmi1* founder lines (T25 and T26) quantified by qRT-PCR at P6 from whole cerebella. (C) Immunohistochemistry on wax sections of P6 cerebella showing increased BMI1 expression in the outer EGL (oEGL) of *Math1-Bmi1* mice (TG) compared with wild-type (WT) mice (line T25 shown). (D) Schematic of the *Gabra6-Bmi1* construct depicting exons 1-8 of *Gabra6* followed by IRES-*Bmi1*. (E) *Bmi1* expression levels, detected by qRT-PCR, in two *Gabra6-Bmi1* founder lines (T3 and T4) at P9 and adult, showing an average of a 2- and 14- to 15-fold increase in expression, respectively, in comparison with wild-type levels. (F) BMI1 protein expression detected by immunohistochemistry in the IGL of transgenic (line T4 shown; TG) but not wild-type animals at P9. (G) Fold increase in *BMI1* expression levels in six individual human primary medulloblastomas (MB-1 to MB-6) in comparison with levels in normal adolescent and adult cerebella, quantified by qRT-PCR. (H) BMI1 protein expression detected by western blot on whole cerebellar extracts from T3 and T4 at P8 and P15, showing downregulation of BMI1 expression in wild-type animals at P15 but high expression maintained in transgenic animals. Bars in B and E show means ± 1 standard deviation (s.d.). Bars in G show individual fold increase in expression per sample. Scale bars: 50 μm. iEGL, inner external granule cell layer; oEGL, outer external granule cell layer; IGL, internal granule cell layer; MB, medulloblastoma; TG, transgenic; WT, wild type; PI, propidium iodide.

Small cerebellar size in *Math1-Bmi1* mice

Despite the appearance of a normal cytoarchitecture, the overall size of the P28 cerebellum appeared smaller in whole-mount sagittal cross-sections of *Math1-Bmi1* mice compared with wild-type littermates (Fig. 2A,B). In support of this observation,

transgenic cerebella were found to weigh significantly less than their wild-type littermates at P22 and P28 (Fig. 2C). The reduction in cerebellar weight did not correlate with a reduction in overall body weight (Fig. 2D) or forebrain weight (data not shown), indicating that *Bmi1* overexpression in GCPs results in a reduction in
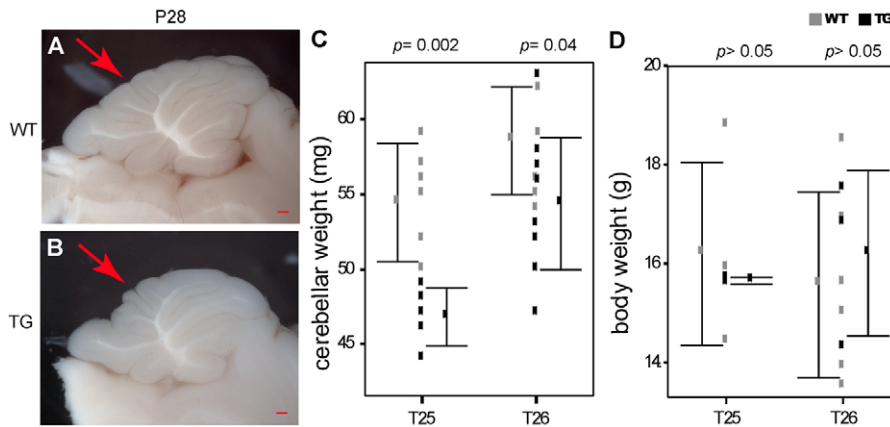
Fig. 2. Cerebellar size is smaller in *Math1-Bmi1* mice compared with wild type. (A,B) Representative examples of the small cerebellar size phenotype (arrows) in *Math1-Bmi1* at P28 shown by views of whole-mount sagittal cross sections of wild-type (A) and transgenic (B) cerebella. (C) Decreased cerebellar weight in T25 and T26 animals in comparison with wild-type littermates. (D) No differences in body weight were observed between genotypes. Rectangles indicate individual values, error bars indicate means ± 1 s.d. Scale bars: 0.5 mm.

cerebellar size. GCP proliferation occurs when the EGL is formed at E14.5, but increases dramatically at birth when sonic hedgehog (*Shh*) expression is detected in the underlying Purkinje cells, and continues until the EGL disappears at around P15 owing to GCP cell cycle exit and migration of cells to the IGL. In order to pinpoint the time point at which the phenotype first manifested, earlier developmental stages were analysed. Crossing of *Math1-Bmi1* mice to *Math1-EGFP* mice (Lumpkin et al., 2003) revealed a timely formation of an EGL as assessed by EGFP expression at E14.5 (Fig. 3A,B). However, at P6, the EGL of transgenic animals was thinner (Fig. 3C-E) and the IGL was reduced in cell density (Fig. 3C,D,F); the reduction in overall cerebellar size was more visibly marked by P8 (Fig. 3G,H), but was not present at the earlier stage of P0 (data not shown). This indicates that the defect is associated with the clonal expansion phase of GCPs, which peaks at around P6 in the mouse (Fujita et al., 1966); therefore, our subsequent analyses were focused around this time point.

Bmi1 overexpression in GCPs reduced cell proliferation

The observed reduction in cerebellar size upon *Bmi1* overexpression was contrary to expectations because previous reports on the effects of *Bmi1* overexpression on stem or progenitor cells had shown an increase in proliferation in the forebrain (He et al., 2009; Fasano et al., 2009; Yadirgi et al., 2011). We set out to investigate the responsible mechanisms and first assessed cell proliferation. To cover the period just preceding the development of a visible phenotype at P6, mice were injected with BrdU at P4 and P5 and analysed at P6 to compare the cumulative number of BrdU-positive cells over a 2 day period. Cells with low BrdU labelling intensity (BrdU^{low} index), indicative of cells that had divided over the 2 day period, were significantly less numerous in the EGL of transgenic mice compared with wild-type littermates (Fig. 4A-D). A reduction in the number of cell cycles undertaken per cell might account for the reduction in cell production between P4 and P6 and the resulting reduction in IGL cell density (Fig. 3F). This would predict that the EGL would disappear earlier in transgenic animals than in wild-type littermates. It has been shown that, at P15, the EGL has almost disappeared in mice due to differentiation of the GCPs (Fujita, 1967). Analysis of EGFP expression at P15 in *Math1-Bmi1* mice crossed with *Math1-EGFP* mice revealed the presence of a thin EGL in both genotypes (Fig. 5A,B). The reduction in granule cell production is therefore not

due to a reduced number of cell cycles and precocious cell cycle exit in GCPs of *Math1-Bmi1* mice.

Next, we considered the possibility that the length of time required for a GCP to complete a cell cycle might have been perturbed by *Bmi1* overexpression, so that GCPs cycle for the normal period of time but complete fewer cell cycles during this time in transgenic compared with wild-type cerebella. The duration of one complete cell cycle has been reported to be between 15-19 hours for GCPs between the ages of P2 and P10 (Fujita, 1967; Yoshioka et al., 1985). Transgenic and wild-type littermates were injected with BrdU at P7 followed by a 30 minute EdU pulse 16 hours later in order to label cells that had completed one cycle in this time frame. The BrdU/EdU double-positive index in the EGL was found to be significantly lower in *Math1-Bmi1* mice than in wild-type littermates (Fig. 5C-G). Although the precise length of the cell cycle (in measure of hours) cannot be estimated with this method, our data suggests that fewer cells have undergone two S-phases in *Math1-Bmi1* mice compared with wild type in the time span of the experiment. We also investigated cell death using the TUNEL and the Annexin V assays at P4 and P6, but detected no differences between *Math1-Bmi1* mice and wild-type littermates (data not shown). Taken together, the lack of precocious cell cycle exit at P15, lack of abnormal levels of cell death, the reduction in the EGL cellularity and the IGL cell density, and a decrease in the BrdU/EdU index raise the possibility that the small cerebellar size phenotype is due to prolonged cell cycle length.

Math1-Bmi1 mice display downregulation of positive regulators of the cell cycle

To gain an understanding of the aberrant control of cell cycle progression at the molecular level, we analysed gene expression changes between wild-type and *Math1-Bmi1* cerebella at P6 using a cell cycle qRT-PCR array. Of the 86 genes analysed, *Ki67* and *PCNA* were significantly downregulated in *Math1-Bmi1* cerebella, confirming the reduction in cell proliferation observed with BrdU and EdU labelling (Fig. 5H). Moreover, several positive regulators of the cell cycle were downregulated, namely the cyclins, with *Ccnb2* (Cyclin B2) reaching statistical significance, as well as *Cks1b* (CDC28 protein kinase 1b), the homologue of the catalytic subunit of the main cell cycle cyclin-dependent kinase in yeast, which is essential for cell cycle progression in somatic cells (Halfter et al.,
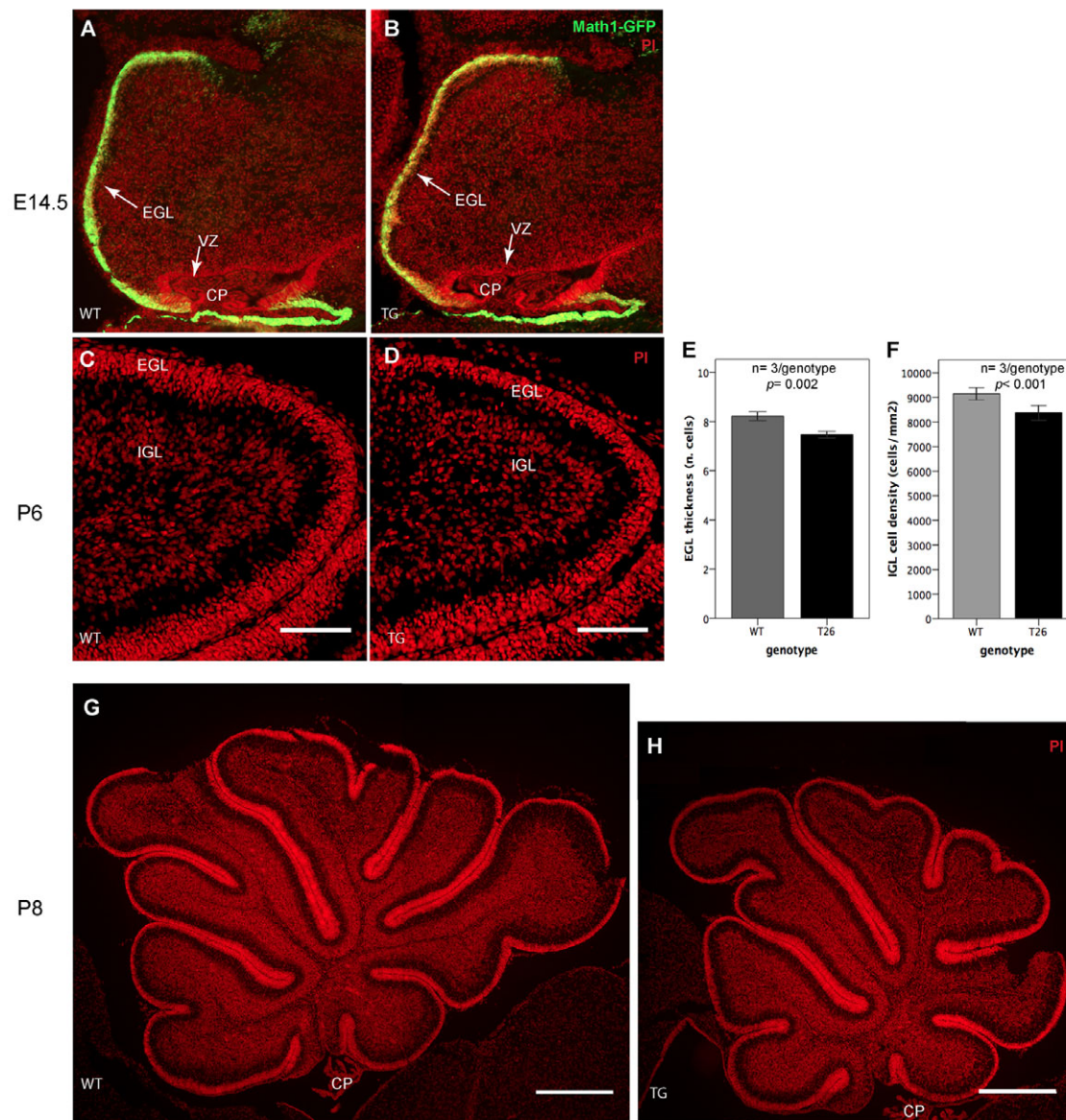
Fig. 3. *Math1-Bmi1* cerebellar size phenotype detected at P6. (A,B) Sagittal sections of E14.5 cerebella showing the formation of an EGL in both *Math1-Bmi1* and wild-type animals. (C,D) Sagittal sections through the cerebellum at P6 showing reduced cellularity in the IGL of transgenic animals in comparison with wild-type littermates. (E) Bar chart showing mean ± 1 standard error of mean (s.e.m.) of the number of cells along the width of the EGL at P7. (F) Bar chart showing the mean cell density ± 1 s.e.m. (number of cells per μm^2) in the IGL of transgenic animals compared with wild-type littermates. (G,H) Sagittal sections at P8 showing reduced overall cerebellar size in transgenic animals compared with wild-type littermates. Scale bars: 0.1 mm in C,D; 0.5 mm in G,H. CP, choroid plexus; EGL, external granule cell layer; IGL, internal granule cell layer; VZ, ventricular zone neuroepithelium; TG, transgenic; WT, wild type; PI, propidium iodide.

2006). The expression of negative regulators of the cell cycle, namely *Cdkn1a* (*p21*), was not changed (Fig. 5H), and *Cdkn2a* (*p16/p19*) was barely detectable in the cerebellum at P6 (data not shown). Interestingly, this effect in GCPs contrasts with the effect of *Bmi1* overexpression in forebrain-derived NSCs, in which *Cdkn1a* and *Cdkn2a* are expressed and downregulated upon *Bmi1* overexpression (Fasano et al., 2009; Yadirgi et al., 2011). These data offer a possible explanation for the different effects on cell proliferation upon *Bmi1* overexpression in the subventricular zone (SVZ) compared with GCPs.

Bmi1 overexpression in GCPs results in reduced expression of DDR genes

A subset of the genes represented on the cell cycle qRT-PCR array were involved in the DDR pathway and their expression was reduced in *Math1-Bmi1* cerebella compared with that in wild-type littermates (Fig. 5I). Particularly, genes involved in the

serine/threonine-protein kinase ATR (ATR)-mediated branch of the DDR pathway were significantly reduced in expression, including *Check1* (checkpoint kinase 1 homologue), a mediator of cell cycle arrest in response to DNA damage and involved in the control of all defined cell cycle checkpoints (Dai and Grant, 2003), and *Rad17* (Rad17 homologue) (Sancar et al., 2004). Other genes affected are involved in DDR-mediated apoptosis [*Ddit3* (DNA-damage inducible transcript 3) (Chen et al., 2008)], proper chromosome alignment in mitosis [*Mad2l1* (MAD2 mitotic arrest deficient-like 1) (Dobles et al., 2000)] and cohesion of sister chromatids after DNA replication [stromal antigen 1 (*Stag1*) (Sancar et al., 2004). Together, downregulation of these genes implies that the GCPs in *Math1-Bmi1* mice might have weakened DDR machinery and therefore be prone to DNA damage and neoplastic transformation. Alternatively, the downregulation of these genes could be a secondary effect in response to other cellular changes induced by *Bmi1* overexpression.
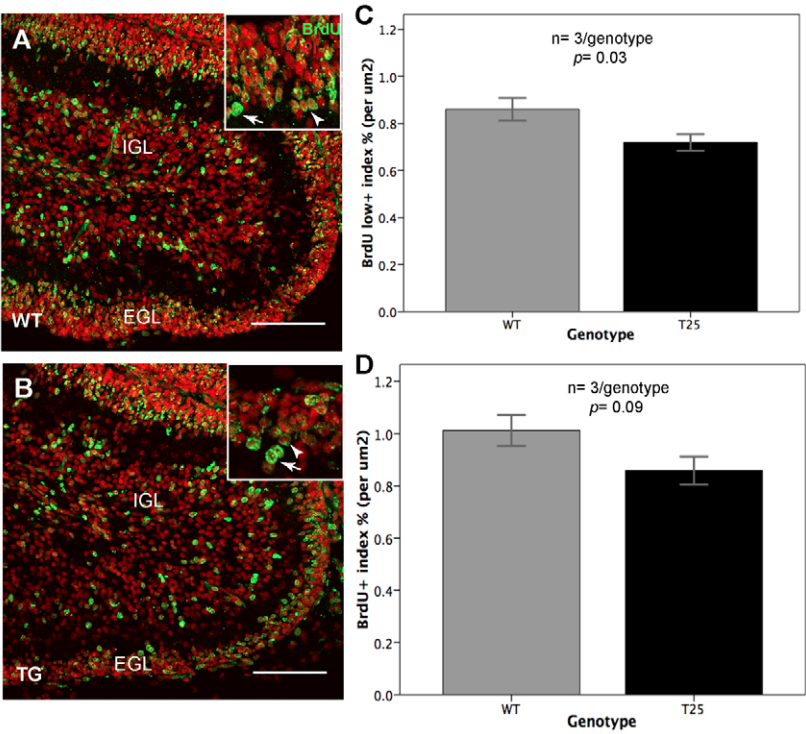
Fig. 4. Cell proliferation is reduced in *Math1-Bmi1* GCPs.
(A,B) Sagittal sections of P6 wild-type and *Math1-Bmi1* cerebella showing cumulative BrdU labelling at P6 upon BrdU injections at P4 and P5. Boxed areas show high-magnification views of BrdU^{high} (arrows) and BrdU^{low} (arrowheads) cells in the EGL. (C) Bar chart showing mean BrdU^{low} index (number of low-intensity BrdU-labelled cells per μm^2 of EGL) ± 1 s.e.m. (D) Overall BrdU index (BrdU-positive cells per μm^2 of EGL) ± 1 s.e.m. Scale bars: 0.1 mm. EGL, external granule cell layer; IGL, internal granule cell layer; TG, transgenic; WT, wild type.

Bmi1 overexpression in GCPs does not induce medulloblastomas, or increase tumour incidence in the *Ptch1*$^{+/-}$ background but induces a low tumour incidence in the *Trp53*$^{-/-}$ background

Cohorts of $n \geq 20$ animals from each line (T25, T26) were aged for at least 1 year. No tumours were detected upon dissection and histological analysis of the brains (Table 1), indicating that *Bmi1* overexpression in GCPs, at the levels achieved, does not initiate medulloblastoma formation.

Because downregulation of DDR genes was detected, we investigated whether *Math1-Bmi1* mice would develop tumours in the presence of additional mutations that destabilise the cell cycle. We generated *Math1-Bmi1* mice on *Trp53*$^{-/-}$ and *Ptch1*$^{+/-}$ genetic backgrounds, which were kept under tumour watch for 6 and 8 months, respectively. *Trp53*$^{-/-}$ mice are highly tumour prone and succumb mainly to lymphomas and sarcomas by 6 months of age (Donehower et al., 1992). Although *TP53* mutations occur in 10% of human medulloblastomas (Ellison, 2002), only one study has so far reported a 2% medulloblastoma incidence in *Trp53*$^{-/-}$ mice on a mixed SV129 (25%); C57Bl/6 (75%) background (Harvey et al., 1993). However, loss of *Trp53* in the mouse is the most powerful predisposing mutation for medulloblastoma formation in

conjunction with other oncogenes (Behesti and Marino, 2009). The most studied medulloblastoma mouse model is the *Ptch1*$^{+/-}$ mouse, which displays abnormally high GCP proliferation leading to medulloblastoma formation between 3 and 6 months of age (Goodrich et al., 1997). The *Math1* enhancer element has previously been shown to drive expression in preneoplastic lesions in *Ptch1*$^{+/-}$ mice (Kessler et al., 2009). One medulloblastoma was found in the *Math1-Bmi1;Trp53*$^{-/-}$ cohort at 4 months of age (4.5%, n=22; Fig. 6A,B) and none in the *Trp53*$^{-/-}$ cohort (0%, n=36). The incidence of medulloblastoma formation was not increased in *Math1-Bmi1;Ptch1*$^{+/-}$ mice (25.7%, n=35) as compared with *Ptch1*$^{+/-}$ littermates (29.2%, n=24; Table 2). Together, these results show that *Bmi1* overexpression in GCPs at the levels achieved does not initiate medulloblastoma formation or enhance progression of preneoplastic lesions into tumours.

Bmi1 overexpression in postmitotic granule cells increases cell survival

Next, we set out to analyse the effect of *Bmi1* overexpression on cell survival under normal and stress conditions, because *Bmi1* overexpression could play a role in promoting cell survival in brain

Table 1. Number, age and sex of aged animals

Animals	*Gabra6-Bmi1* (T3)	*Gabra6-Bmi1* (T4)	*Math1-Bmi1* (T5)	*Math1-Bmi1* (T6)
No. MB in total number of cohort	0/22	0/29	0/25	0/25
No. animals >1 year	14	28	21	24
No. animals >1.5 years	4	15	3	3
Age of oldest animal in colony	2 years 4.5 months	2 years 10 days	1 year 8 months	1 year 9 months
Males per colony	11/22 (50%)	13/29 (45%)	12/25* (49%)	14/25 (56%)
Females per colony	11/22 (50%)	16/29 (55%)	12/25* (49%)	11/25 (44%)

*One unknown. MB, medulloblastoma.

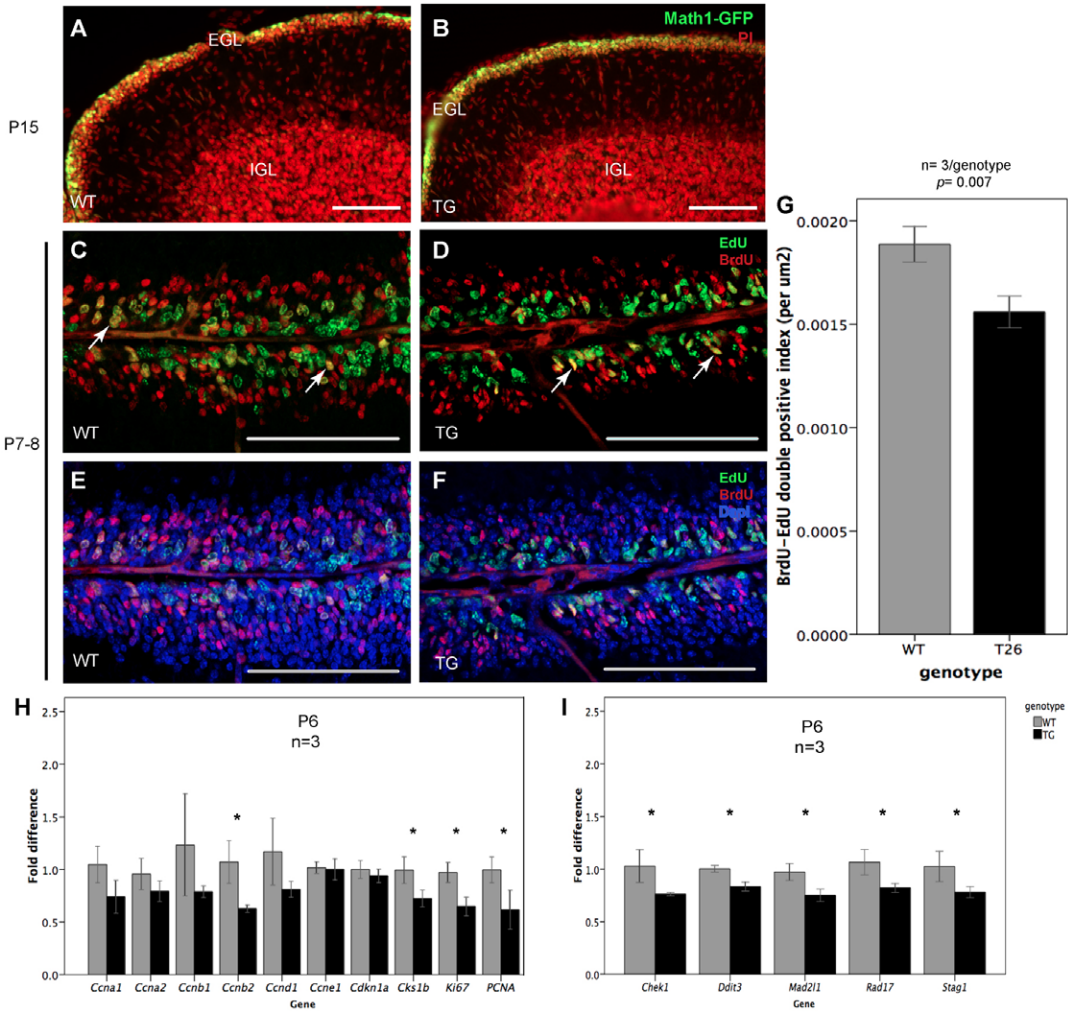**Fig. 5. Cell cycle length is increased in *Math1-Bmi1* GCPs.** (A,B) Sagittal sections at P15 of *Math1-Bmi1* × *Math1-EGFP* cerebella (TG) and *Math1-EGFP* littermate control (WT), showing the presence of an EGL and Math1-GFP-positive cells in both genotypes. (C,D) Sagittal sections of EGL showing EdU/BrdU double labelling at P8 in wild-type (C) and *Math1-Bmi1* (D) cerebella. Arrows show examples of double-positive cells. (E,F) Images in C and D with DAPI overlay for labelling of nuclei. Scale bars: 0.1 mm. (G) Bar chart showing a decrease in the mean EdU/BrdU double-positive index (double-positive cells per μm^2 of EGL) ± 1 s.e.m. in transgenic animals compared with wild-type littermates. (H,I) Quantification of gene expression changes by qRT-PCR array at P6, expressed as mean fold change in comparison with wild type ± 1 s.d., showing a trend of downregulation in positive regulators of the cell cycle (H) and DDR pathway genes (I). Asterisks indicate significant downregulation compared with wild type. EGL, external granule cell layer; IGL, internal granule cell layer; TG, transgenic; WT, wild type; PI, propidium iodide.

tumours. Recently, a study showed decreased neuronal survival in the absence of *Bmi1* (Chatoo et al., 2009) owing to a weakened antioxidant defence system, prompting the question of whether *Bmi1* overexpression enhances cell survival in the granule cell lineage. Moreover, *Bmi1*$^{-/-}$ mice display progressive cerebellar degeneration with age, partly due to increased ROS levels (Liu et al., 2009). Cerebellar cultures established from the *Gabra6-Bmi1* lines were chosen for cell survival studies in vitro because cerebellar granule cells differentiate soon after plating in culture and the *Gabra6* construct drives *Bmi1* expression in postmitotic granule cells. BMI1 overexpression in cultures established from *Gabra6-Bmi1* cerebella at P7 was confirmed by immunocytochemistry (Fig. 7G,H). These cultures displayed differentiation soon after plating, as shown by almost complete lack of BrdU-positive cells on day in vitro (DIV) 1-3, similar to wild-type cultures (Fig. 7A-F). On day 3, the number of glial fibrillary acidic protein (GFAP)-positive astrocytes started to increase, whereas overall cell survival decreased (Fig. 7E,F). Cell survival was quantified at DIV4 by counting the number of DAPI-positive live cells with distinguishable nucleoli. Cell survival was also assessed with the alamar blue assay (supplementary material Fig. S1). *Gabra6-Bmi1* cultures were on average significantly more numerous than wild-type cultures (Fig. 7I, see average) and displayed a significantly lower GFAP index (Fig. 7J, see average).

Table 2. Medulloblastoma in transgenic mice crossed with *Trp53*$^{-/-}$ and *Ptch1*$^{+/-}$

| Animals	*Gabra6-Bmi1* (T4) × *Trp53*$^{-/-}$	*Math1-Bmi1* (T25, T26) × *Trp53*$^{-/-}$	*Math1-Bmi1* (T25, T26) ×		
			Trp53$^{-/-}$	*Ptch1*$^{+/-}$	*Ptch1*$^{+/-}$
No. MB in total number of cohort (percentage)	1/20 (5%)	1/22 (4.5%)	0/36 (0%)	9/35 (25.7%)	7/24 (29.2%)
No. animals <6 months	9	15	26	2	3
No. animals >6 months	11	6	9	19	8
No. animals >8 months	0	1	1	14	13

MB, medulloblastoma.

Increased GFAP expression has been detected under stress conditions and is considered a marker of normal and reactive astrocytes (Chen and Swanson, 2003; Wu and Schwartz, 1998). The difference in cell survival between *Gabra6-Bmi1* and wild-type littermate cultures set up simultaneously was most apparent in cultures that displayed a higher GFAP index (Fig. 7I,J, preps 2 and 3). These findings suggest that *Gabra6-Bmi1* cultures display improved cell survival under general culture stress compared with wild-type cultures.

To test whether postmitotic granule cells in which *Bmi1* is overexpressed displayed increased resistance to stress, we employed the glutamate assay, which induces necrotic and apoptotic cell death owing to excitotoxicity in granule cells (Ankarcrona et al., 1995), and the hypoxia-normoxia assay, which is highly relevant for modelling a tumour environment.

Cerebellar granule cells isolated at P7-P8 are only responsive to glutamate excitotoxicity after 1 week in culture (Frandsen and Schousboe, 1990). We found that glutamate (100 µM) treatment of *Gabra6-Bmi1* and wild-type cultures at DIV7 resulted in a significant decrease in cell survival. The number of DAPI-positive live cells decreased to 22±8% (of non-treated) in wild-type cultures, whereas survival in *Gabra6-Bmi1* cultures was 48±16% of non-treated cells (Fig. 7K), indicating a significant improvement upon BMI1 overexpression.

The hypoxia-normoxia assay was used to test the hypothesis that BMI1 overexpression reduces oxidative stress in the cerebellar granule cell lineage. Cerebellar granule cell cultures were incubated for 3 hours at 0.2% hypoxia at DIV2, followed by 24 hours at normoxia. Although transgenic cultures displayed an increased trend in survival (75±14% in *Gabra6-Bmi1* cultures

Fig. 6. Medulloblastomas in *Math1-Bmi1;Trp53$^{-/-}$* and *Gabra6-Bmi1;Trp53$^{-/-}$* mice and enrichment of human medulloblastomas with the *BMI1^{high} TP53^{low}* molecular profile in Group 4. Medulloblastoma arose with low frequency in both *Math1-Bmi1;Trp53$^{-/-}$* (A and high magnification in B) and *Gabra6-Bmi1;Trp53$^{-/-}$* (C and high magnification in D) mice. Morphological analysis revealed tumours composed of small round blue cells with moderately pleomorphic and hyperchromatic nuclei and scant cytoplasm (B,D). Tumours were, in places, sharply demarcated from the surrounding cerebellum (A). However, focal spreading into the leptomeningeal space and the molecular layer was also seen (C). Scale bar: 250 m (A,C) and 125 m (B,D). (E) *BMI1* overexpression, relative to median fetal cerebellar levels of expression, occurred across all subgroups of medulloblastoma. *BMI1* was most highly expressed in Group 4 (>3-fold versus median fetal cerebella), followed by Group 3 (>1.93-fold), then the SHH (>1.92-fold) and WNT (>1.60-fold) subgroups. Lowest TP53 expression was found in Group 4. (F,G) A statistically significant enrichment of Group 4 medulloblastoma was found across tumours expressing higher levels of *BMI1* and low levels of *TP53* (F,G; *P*<1.0×10^{-4}). CB, cerebella; MBS, medulloblastoma.
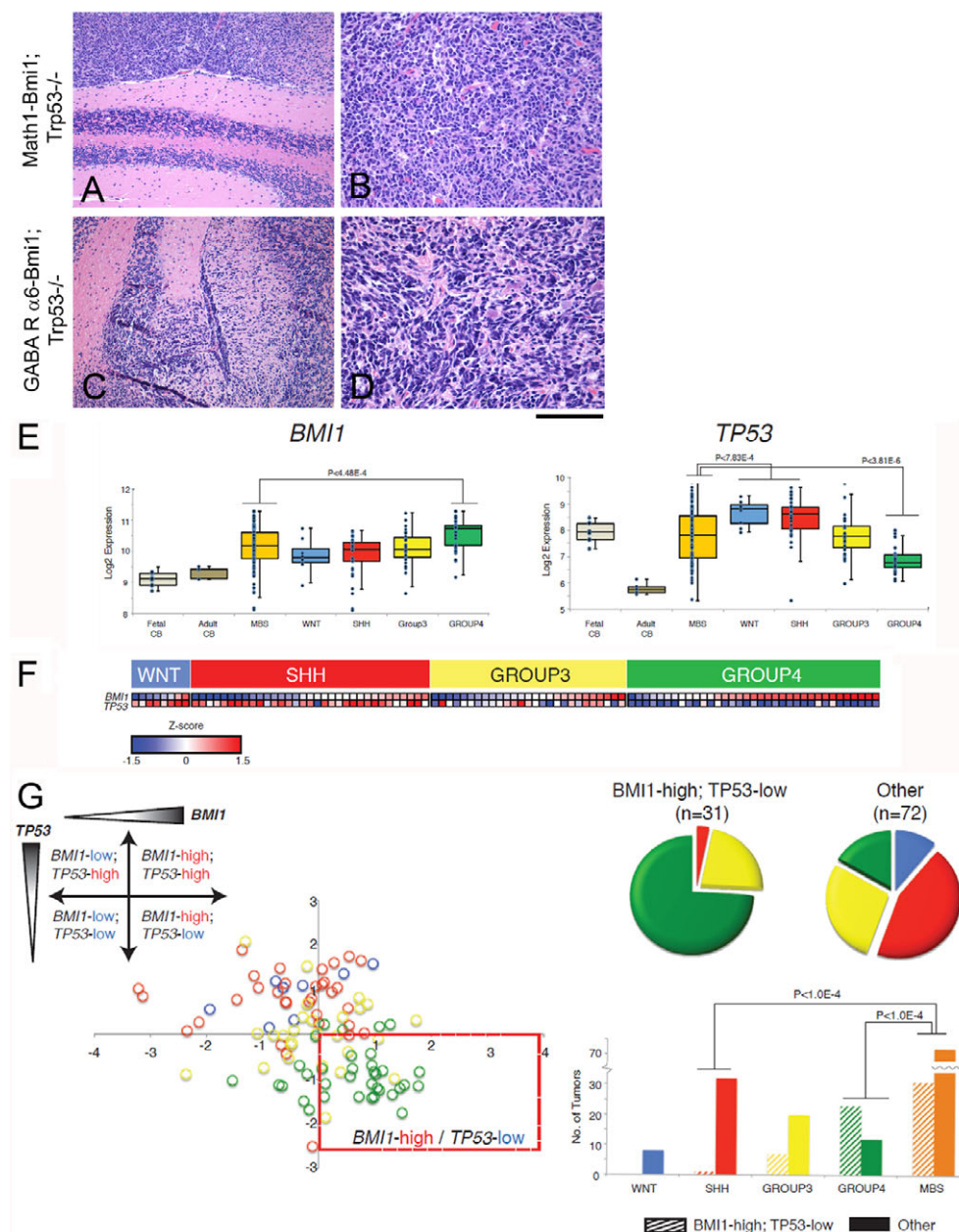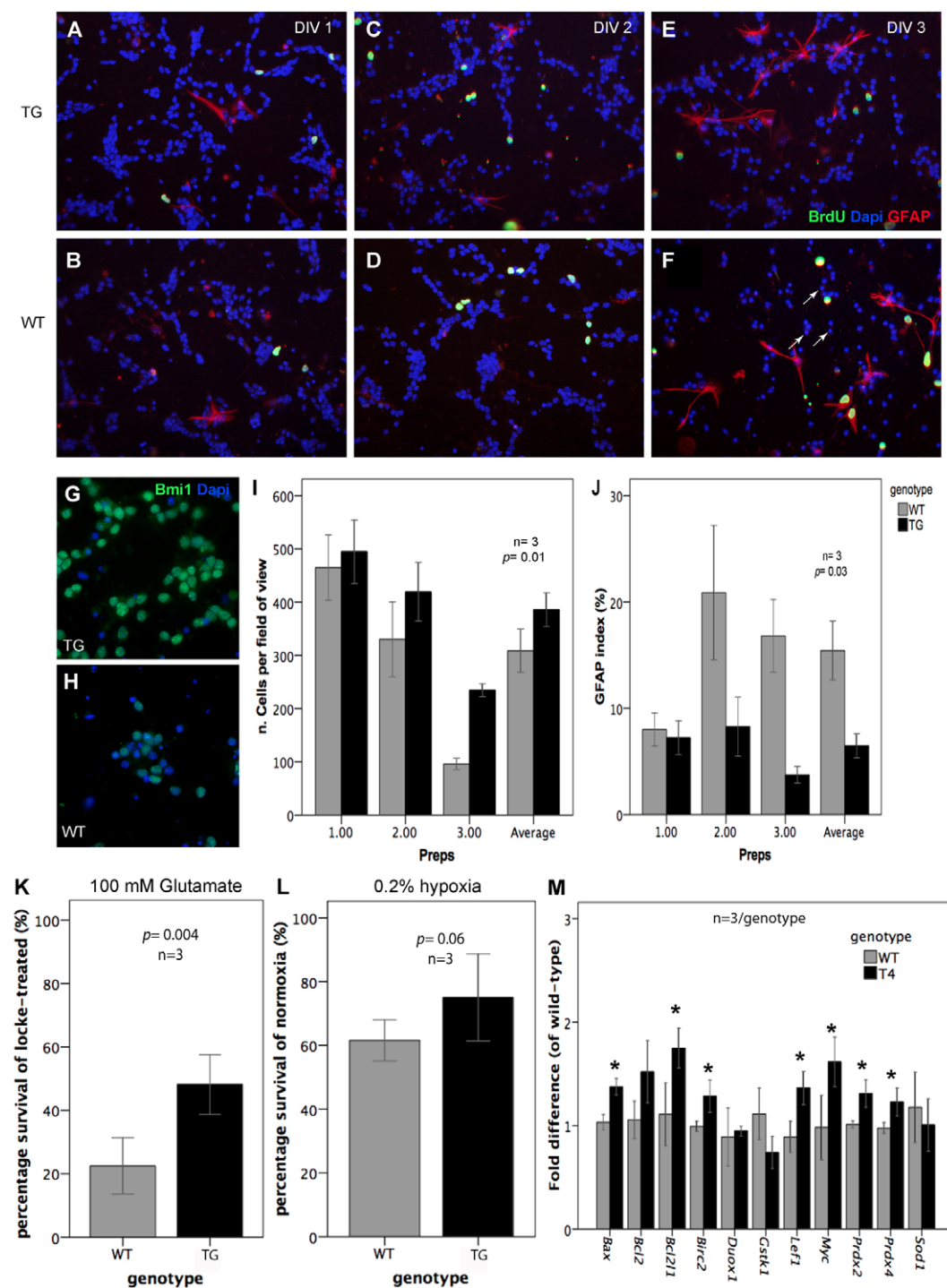
Fig. 7. BMI1 overexpression in postmitotic granule cells improves survival in response to stress and induces gene expression changes in the mitochondrial cell death pathway. (A-F) BrdU labelling and GFAP expression in *Gabra6-Bmi1* and wild-type cultures at DIV1 (A,B), DIV2 (C,D) and DIV3 (E,F). Arrows highlight DAPI+ condensed nuclei. (G,H) BMI1 expression in *Gabra6-Bmi1* and wild-type cultures shown by immunocytochemistry at DIV4. (I) Bar chart showing mean DAPI+ live cells per culture (prep) ±1 s.d. and average ± 1 s.e.m. of three cultures in *Gabra6-Bmi1* and wild-type preps. (J) Bar chart showing the mean GFAP index (number of GFAP+ cells per total number of cells) ± 1 s.d. per culture and the average ± 1 s.e.m. of three cultures in *Gabra6-Bmi1* and wild-type preps. (K) Percentage cell survival ± 1 s.e.m. upon glutamate treatment (number of DAPI+ live cells in glutamate treated over Locke treated cultures) in *Gabra6-Bmi1* and wild-type preps, 24 hours post glutamate treatment at DIV8. (L) Percentage cell survival ± 1 s.e.m. upon 0.2% hypoxia treatment (number of DAPI+ live cells in hypoxia-treated over normoxia-treated cultures) in *Gabra6-Bmi1* and wild-type preps at DIV3, 24 hours post hypoxia. (M) Relative expression levels of genes involved in the mitochondrial cell death pathway, cell survival and oxidative stress quantified by qRT-PCR array in *Gabra6-Bmi1* cerebellar cultures at DIV3 in comparison with wild-type cultures. Bar chart shows mean ± 1 s.d. fold change of gene expression in relation to wild-type levels. Asterisks indicate significant upregulation. DIV, days in vitro; TG, transgenic; WT, wild type.

versus 61.5±6% in wild-type cultures), this data did not reach statistical significance (Fig. 7L). To further investigate a possible effect on the antioxidant defence system in granule cells upon BMI1 overexpression, we compared ROS production in cultures from *Gabra6-Bmi1* and wild-type cerebella. There was no difference in endogenous H_2DCFDA levels, indicative of ROS production, between genotypes at DIV2 in normoxia (Fig. 8A). Although ROS production increased after incubation in hypoxia, there were no differences in ROS production between genotypes

upon hypoxia treatment (Fig. 8B), confirming that BMI1 overexpression in granule cells does not protect against oxidative stress. Finally, we investigated the effect of *BMI1* overexpression on ROS production in a human medulloblastoma cell line. DAOY cells express high levels of BMI1 (Leung et al., 2004) and, upon siRNA-mediated knockdown of *BMI1* (Fig. 8C), cell numbers were significantly reduced on DIV2 compared with numbers in scrambled-siRNA-treated cultures (Fig. 8D). ROS production was similar between *BMI1*-siRNA- and scrambled-siRNA-treated
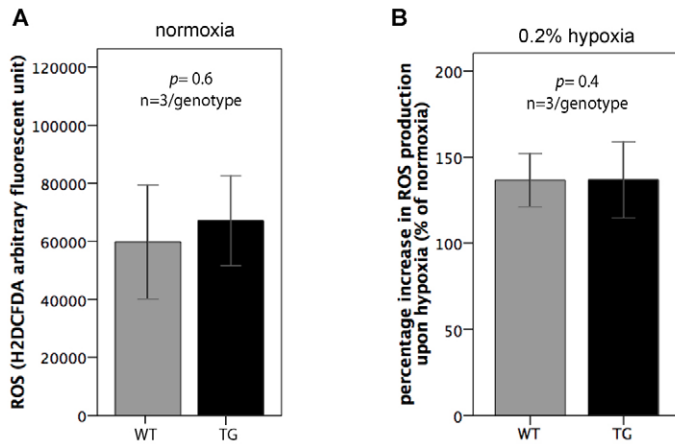
Fig. 8. High levels of BMI1 expression in the granule cell lineage or DAOY cells does not alter ROS levels. (A) Mean fluorescent intensity of $H_2DCFDA \pm$ s.e.m., indicative of intracellular ROS levels, under normoxic conditions at DIV2 in *Gabra6-Bmi1* and wild-type cultures. (B) Mean ± 1 s.e.m. percentage increase (of normoxia) in ROS production upon 0.2% hypoxia treatment at DIV2 in *Gabra6-Bmi1* and wild-type cultures. (C) qRT-PCR quantification of *BMI1* expression levels in DAOY cells, 48 hours after *BMI1* siRNA and scrambled siRNA treatment. (D) Mean ± 1 s.d. number of cells at 48 hours post *BMI1* siRNA and scrambled siRNA treatment of DAOY cells. (E) Mean fluorescence intensity of $H_2DCFDA \pm 1$ s.e.m. in *BMI1*-siRNA- and scrambled-siRNA-treated DAOY cells. TG, transgenic; WT, wild-type.
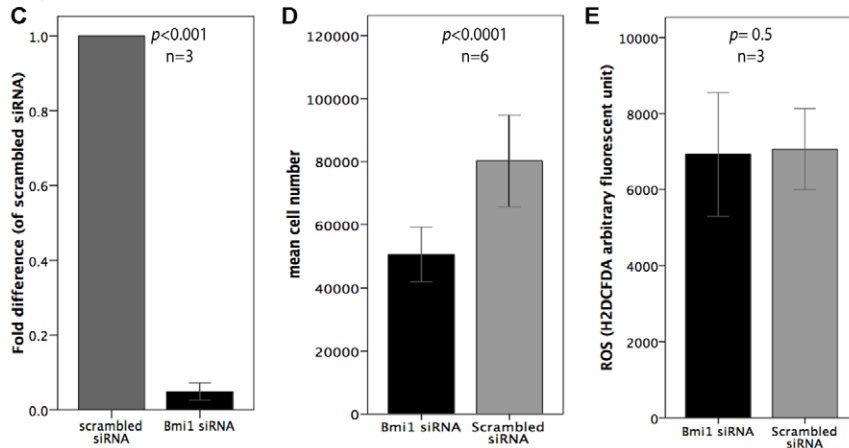
cells (Fig. 8E), confirming that BMI1 overexpression in mouse cerebellar granule cells or in a human medulloblastoma cell line with high levels of *BMI1* does not alter ROS production. In conclusion, BMI1 overexpression improves granule cell survival during general culture stress and upon glutamate excitotoxicity, but has little effect on ROS production.

Gene expression changes that are associated with *Bmi1* overexpression and improved granule cell survival

In order to examine the molecular pathway(s) responsible for improving granule cell survival in *Gabra6-Bmi1* cultures, we analysed gene expression changes by qRT-PCR arrays in DIV3 cerebellar cultures. This time point was chosen because it was 1 day prior to the detection of a significant difference in survival between *Gabra6-Bmi1* and wild-type cerebellar cultures (Fig. 7I). The qRT-PCR arrays contained primers for genes involved in the regulation of oxidative stress and cell death or survival. Of 172 genes analysed, we detected increased expression of genes in the B-cell lymphoma 2 (Bcl2) family of pro- and antiapoptotic genes (*Bax*, *Bcl2l1*), the Lef-Myc pathway, and members of the peroxiredoxin family of antioxidant enzymes (*Prdx1*, *Prdx4*). We did not detect changes in several antioxidant genes previously shown to be deregulated in *Bmi1*$^{-/-}$ mice, such as *Duox1*, *Nqo*, *Sod1* and *Sod2* (Fig. 7M and data not shown).

Bmi1 overexpression in postmitotic granule cells does not lead to medulloblastoma formation but induces a low tumour incidence in a *Trp53*$^{-/-}$ background

Although cell cycle re-entry of postmitotic neurons and neoplastic transformation seem unlikely, a study showed that retinal horizontal cells that harbour *Rb*$^{-/-}$; *p107*$^{+/-}$; *p130*$^{-/-}$ mutations re-enter the cell cycle and yield metastatic retinoblastomas (Ajioka et al., 2007). We kept the *Gabra6-Bmi1* mice under observation for tumour formation. Cohorts of $n \geq 20$ animals from each line (T3, T4) were aged for at least 1 year. Neurological symptoms associated with medulloblastoma formation were not observed and no tumours were detected upon dissection and histological analysis of the brains (Table 1). The *Gabra6-Bmi1* mice were also crossed with *Trp53*$^{-/-}$ mice and aged for 6 months. One mouse displayed behavioural traits associated with cerebellar pathology, such as loss of balance. Upon dissection, a medulloblastoma tumour was detected in the ventral hemisphere (5%, $n=20$; Fig. 6C,D). No tumours were observed in *Gabra6-Bmi1* mice on a *Trp53*$^{+/-}$ background (0%, $n=27$) or in *Trp53*$^{-/-}$ mice alone (0%, $n=36$; Table 2).

Tumours with a *BMI1*^{high} *TP53*^{low} molecular profile are significantly enriched in Group 4 human medulloblastomas

Genome-wide expression analyses have substantially advanced our understanding of the molecular pathogenesis of human

medulloblastoma, identifying four distinct subgroups affecting prognosis and predicting response to therapy (Kool et al., 2008; Northcott et al., 2011; Pomeroy et al., 2002; Thompson et al., 2006). Two subgroups, characterised by activation of WNT and SHH pathways, respectively, are associated with a more favourable prognosis, whereas groups 3 and 4 are less well defined at the molecular level but are clinically characterised as a more aggressive disease with poorer outcome (Taylor et al., 2012).

To bridge our mouse models of *Bmi1* overexpression with the human disease, we analysed *BMI1* and *TP53* expression in a data set derived from 103 primary human medulloblastomas and 14 normal cerebella (fetal *n*=9; adult *n*=5), profiled on Affymetrix Exon 1.0ST arrays. We observed *BMI1* overexpression in 54% of tumours, relative to median fetal cerebellar levels of expression, which occurred across all subgroups of medulloblastoma. *BMI1* was most highly expressed in Group 4 (>3-fold versus median fetal cerebella), followed by Group 3 (>1.93-fold), SHH (>1.92-fold) and WNT (>1.60-fold) subgroups (Fig. 6E). Because medulloblastoma formation could not be initiated by *Bmi1* overexpression alone, we examined the expression pattern of human medulloblastomas with relative *BMI1* overexpression and reduced *TP53* expression (*BMI1^high^*; *TP53^low^*) because a low incidence of medulloblastoma was observed in *Math1-Bmi1* and *Gabra6-Bmi1* mice on a *Trp53* null background. A statistically significant enrichment of Group 4 medulloblastoma was found across tumours expressing higher levels of *BMI1* and low levels of *TP53* (Fig. 6F,G; $P<1.0\times10^{-4}$), raising the possibility that this combination of mutations plays a role in the pathogenesis of Group 4 human medulloblastomas specifically.

DISCUSSION

Bmi1 is a potent inducer of NSC self-renewal in vitro (Fasano et al., 2007; He et al., 2009; Molofsky et al., 2003) and in vivo (Fasano et al., 2009; Yadirgi et al., 2011). Its ability to induce NSC self-renewal could be exploited to enhance repair and regeneration, yet its abnormally high expression levels in various cancers, including medulloblastoma, raises the question of whether it is oncogenic if overexpressed in the wrong cell at the wrong time, and whether it can initiate tumour formation. We generated and analysed transgenic mice that overexpress *Bmi1* at different stages of development and maturation of cerebellar granule cells, a cell type shown to be a cell of origin for mouse medulloblastomas. We found no evidence for an oncogenic role for *Bmi1* in the developing cerebellum when overexpressed at the levels described. Instead, it decreased proliferation of GCPs, leading to a reduction in cerebellar size. Although loss of *Bmi1* has also been reported to cause a reduction in GCP proliferation in *Bmi1^-/-^* mice, our results show that *Bmi1* overexpression in GCPs acts through a different mechanism. Instead of BMI1 repression of cell cycle inhibitors *p16*, *p19* and *p21* (Fasano et al., 2007; Subkhankulova et al., 2010), which are responsible for many of the lymphoid and neurological defects detected in *Bmi1^-/-^* mice or detected upon *Bmi1* overexpression in SVZ NSCs or progenitors (Fasano et al., 2009; Yadirgi et al., 2011), we detected reduced expression of genes associated with promoting the cell cycle, including downregulation of the cyclins. This effect could be direct or due to compensatory mechanisms initiated to counteract the increased *Bmi1* levels. Moreover, whereas increased proliferation in the study of Fasano et al. was induced by high levels

of *Bmi1* overexpression (~500- to 1500-fold increased expression) (Fasano et al., 2009), we have previously reported that a 2-fold increase in *Bmi1* levels in NSCs and progenitors in the forebrain also leads to increased proliferation (Yadirgi et al., 2011). We therefore favour the interpretation that BMI1 induces distinct cellular responses depending on the level and the timing of overexpression. This is in agreement with the fact that some reports show repression of p16 and p19 whereas others show no change in the expression of these genes upon manipulation of BMI1 expression, suggesting that the profile of the cell at the time of BMI1 expression dictates the outcome.

In addition to cell cycle genes, we detected changes in DDR pathway genes, in agreement with other recent studies reporting BMI1 enrichment in γ-irradiated glioblastoma multiforme cell lines, leading to decreased sensitivity of these cells to radiation (Facchino et al., 2010). We detected downregulation of *Check1* and *Rad17* in *Math1-Bmi1* cerebella, both of which act in the ATR-mediated DDR pathway and, together with the apoptotic machinery, are often repressed during neoplastic transformation (Jackson and Bartek, 2009). Although several DDR pathway genes were repressed in *Math1-Bmi1* mice, crossing onto a *Ptch^+/-^* background did not increase the medulloblastoma incidence of the *Ptch^+/-^* mice and crosses onto a *Trp53*-deficient background induced a low tumour incidence. The lack of increased tumour incidence in *Math1-Bmi1;Ptch1^+/-^* mice is probably due to repressed expression of the cyclin genes and cell proliferation in *Math1-Bmi1* cerebella alone. In addition, it could be due to the lack of an effect on cell differentiation in *Math1-Bmi1* mice. It has been shown that the majority of early preneoplastic lesions in *Ptch1^+/-^* mice fail to progress into tumours because they undergo differentiation (Kessler et al., 2009). Alternatively, it could be due to the low level of *Bmi1* overexpression achieved in our mice. We and others have not been able to obtain transgenic lines that overexpress *Bmi1* at very high levels (He et al., 2009) in proliferating cells, indicating that perhaps high levels of *Bmi1* overexpression are incompatible with embryonic development. We showed here that *Bmi1* overexpression improves cell survival in vitro during normal culture and in response to glutamate excitotoxic stress. Gene expression studies show the expression of several glutamate receptors in medulloblastoma cell lines (Yoshioka et al., 1996) and in vivo proton magnetic resonance spectroscopy studies have revealed high levels of glutamate in primary medulloblastomas (Davies et al., 2008). Therefore, BMI1-conferred enhanced survival in a glutamate-rich environment might provide a growth advantage in medulloblastoma pathogenesis. We also tested the effect of *Bmi1* overexpression on granule cell survival in response to oxidative stress. Recent studies have highlighted a role for BMI1 in antioxidant defence systems and in counteracting intracellular ROS levels in normal tissues (Chatoo et al., 2009; Liu et al., 2009). The effect of *Bmi1* overexpression in normal and pathogenic cell survival by counteracting ROS levels or the regulation of antioxidant genes have not been tested previously. Tumour cells are highly prone to the accumulation of ROS because of high rates of cell proliferation and metabolism, and therefore acquirement of a cell-autonomous capacity to reduce ROS levels is an important advantage in tumour progression (Schafer et al., 2009). However, we did not detect any significant changes in survival or ROS levels in response to hypoxia in cultures established from *Gabra6-Bmi1*

and wild-type cerebella. Moreover, *BMI1* knockdown did not result in alterations in ROS levels in DAOY cells. Although ROS levels are increased in *Bmi1*−/− mice, a recent study has shown that ROS levels are not affected by *BMI1* knockdown in glioblastoma cell lines (Facchino et al., 2010), suggesting that the effect of BMI1 on ROS levels might also vary between cell types and normal and pathologic states.

Although BMI1 expression is downregulated in the cerebellum as development proceeds, low levels are still detected post GCP proliferation. The cerebellar degeneration phenotype in *Bmi1*−/− mice is rescued by antioxidant treatment or loss of *Chek2* or *p19* and *p16* (Liu et al., 2009; Molofsky et al., 2005), but only partially, indicating that other pathways are also at work. We have identified upregulation of additional genes relevant for cell survival upon BMI1 overexpression in cerebellar granule cells. An upregulation in the expression of *Bax*, *Bcl2l1*, *Birc2*, *Lef1* and *Myc* was detected in *Gabra6-Bmi1* cerebellar cells. The functional translation of upregulation of *Bax* together with *Bcl2l1* is not clear because these have opposite effects on apoptosis (Zinkel et al., 2006). *Myc* is a Lef1 target gene; Lef1 has been found to promote epithelial cell survival during tooth morphogenesis (Sasaki et al., 2005), granulocyte survival (Skokowa et al., 2006) and lymphoma cell survival (Spaulding et al., 2007). Together, these results suggest that *Bmi1* can act through Myc-Lef1 and/or Bcl2 family of survival genes to modulate cell survival.

Overexpression of *Bmi1* in a *Trp53*-deficient background induced medulloblastoma, albeit at a very low frequency. Interestingly, however, an enrichment of tumours with relatively high expression of *BMI1* and low expression of *TP53* was found in Group 4 human medulloblastomas. It will therefore be interesting and clinically relevant to assess the level and stage at which *Bmi1* is first upregulated during the oncogenic process and employ a conditional mouse model approach that facilitates the switching on and off of the expression of extra copies of *Bmi1* at various developmental and oncogenic stages to gain further understanding of the role of BMI1 in medulloblastoma pathogenesis.

In summary, our findings show that the effect of BMI1 overexpression is dependent on levels of overexpression and the ontogenic stage of the cell. Importantly, the results presented here highlight a role for BMI1 overexpression in neuronal survival under stress conditions in vitro. It will be of interest to assess whether a similar effect on neuronal survival can be seen in vivo, which could lay the basis for future potential therapeutic exploitation of this observation.

METHODS
Transgenic and knock-out mouse lines
All experiments were carried out in compliance with UK home office regulations. For *Math1-Bmi1*, the GFP sequence in the BgnGFP vector (Lumpkin et al., 2003) was replaced with a full-length mouse *Bmi1* cDNA (3.1 kb) between the *Nco*I and *Xho*I restrictions sites. *Bmi1* expression was therefore driven by the 1.4 kb *Math1* enhancer followed by 144 nucleotides on the 3′ end and the β-globin basal promoter (Fig. 1A). For *Gabra6-Bmi1*, the *Sph*I-*Ada*I fragment of the *pmα6IRES-LacZ6* vector (Bahn et al., 1997) containing exons 1-8 of the *Gabra6* subunit gene was ligated to the *Bmi1* full-length cDNA preceded by the *Ada*I-*Nco*I fragment

of IRES in a pΛCYC184 vector (Fig. 1C). Transgenic mice were generated according to standard procedures at University Hospital Zurich. Founder mice were bred with wild-type C57Bl/6 mice and transgenic animals were identified by PCR genotyping. *Math1-GFP* mice on a C57Bl/6 background were obtained from Jane Johnson, Southwestern Medical Centre, University of Texas, TX. *Ptch1*[tm1Mps]/J mice on a mixed background were purchased from the Jackson Laboratory (Goodrich et al., 1997). *Trp53*+/− mice on a C57Bl/6 background were obtained from CRUK London (Donehower et al., 1992). Primers for genotyping were as follows: *Math1-Bmi1*: forward 5′-AGAGCGGCTGACAATAGAGG-3′ reverse 5′-TGGTTTTGTGAACCTGGACA-3′ (489 bp), *Math1-Gabra6*: forward 5′-AGCATCAGCTGACGGGTGAG-3′, reverse 5′-CAGTGCCACGTTGTGAGTTGATAG-3′ (~600 bp), *Math1-GFP*: forward 5′-GGTGAGCGCACTCGCTTTCAG-3′, reverse 5′-TCCTTGAAGAAGATGGTGCG-3′ (700 bp), *Ptch1*[tm1Mps]/J: mutant allele forward 5′-GCCCTGAATGAACTGCAGGACG-3′, mutant allele reverse 5′-CACGGGTAGCCAACGCTATGTC-3′, wild-type allele forward 5′-CTGCGGCAAGTTTTTGGTTG-3′, wild-type allele reverse 5′-AGGGCTTCTCGTTGGCTACAAG-3′ (mutant band 479 bp, wild-type band 200 bp), *Trp53*+/−: neo primer 5′-GCTCTGATGCCGCCGTGTTCCG-3′, wild-type allele forward 5′-GTGTTTCATTAGTTCCCCACCTTGAC-3′, wild-type reverse 5′-ATGGGAGGCTGCCAGTCCTAACCC-3′ (mutant band 862 bp, wild-type band 310 bp).

Gene expression analysis by qRT-PCR
RNA from P6-P7 or adult cerebellum was extracted using TRIzol (Invitrogen, UK), DNase-treated using Amp Grade DNase I (Invitrogen, UK), and purified using Qiagen micro columns (Qiagen, UK), all according to the manufacturers' descriptions. RNA from human primary medulloblastomas was kindly provided by Francesca Menghi and Jonathan Ham (Institute of Child Health, London, UK). RNA from DAOY cells and mixed cerebellar cultures were extracted using the Qiagen RNeasy Micro Kit (Qiagen, UK) according to the manufacturer's descriptions. For *Bmi1/BMI1* expression analysis, first-strand cDNA was synthesised with the Superscript III Reverse Transcriptase kit (Invitrogen, UK), using anchored OligodT primers (Invitrogen, UK). Expression levels were detected on an Applied Biosystems 7500 Real-Time PCR machine using the default PCR programme and TaqMan Gene Expression Master Mix and primers (Hs00180411_m1, Hs99999903_m1, Mm00776122_gH, Mm0067939_S1). For the Oxidative Stress and Signal Transduction PathwayFinder (SABiosciences, UK) PCR-array analyses, first-strand cDNA was synthesised with RNA from DIV3 cerebellar cultures with the RT^2 PCR Array First Strand Kit (SABiosciences, UK) according to the manufacturer's descriptions. Cell cycle genes were analysed on a Cell Cycle PCR array (SABiosciences, UK), using RNA from P6 cerebella and cDNA prepared as described above for PCR array experiments. All analyses were performed on three biological replicates per genotype. All data were expressed as $2^{-\Delta\Delta Ct}$ fold difference of wild-type littermates.

Western blotting, immunohistochemistry and detection of EdU
The following primary antibodies were used: mouse anti-BMI1 (1:100 for immunohistochemistry, 1:200 for western blot, Millipore clone F6), rabbit anti-GFAP (Dako, 1:1000), mouse anti-BrdU

(Sigma, Clone BU33, 1:500), mouse anti-BrdU (Dako, 1:80) and anti-Gapdh (1:1000 Abcam).

The following secondary antibodies were used: anti-mouse Alexa-Fluor-488, anti-mouse Alexa-Fluor-546, anti-rabbit Alexa-Fluor-546 (1:200, Invitrogen, UK) and HRP-conjugated anti-mouse (1:5000, Santa Cruz Biotechnology).

Western blotting was carried out according to standard protocols.

For immunohistochemistry on frozen sections, brains were fixed overnight in 4% paraformaldehyde (PFA) at 4°C, cryoprotected in 20% sucrose (Fisher, UK) and sectioned at 12 µm thickness. BMI1 was detected with the Vector M.O.M. immunodetection kit (Vectorlabs Inc.) according to the manufacturer's description with the exception of BMI1 antibody incubation being performed overnight at 4°C. For BrdU/EdU immunohistochemistry, sections were permeabilised in 0.5% Triton-PBS for 50 minutes, blocked in 3% BSA for 1 hour, and incubated for 30 minutes with Click-iT® reaction according to the manufacturer's description to first detect EdU (Click-iT® EdU Alexa Fluor® 488 Imaging Kit, Invitrogen, UK). Sections were incubated in 0.1 M glycine pH 7.4 for 30 minutes, followed by incubation in 2 M HCl for 30 minutes at 37°C, then blocked in 10% horse serum for 1 hour, incubated with anti-BrdU (Sigma, Clone BU33) overnight at 4°C, and finally incubated with Alexa-Fluor-546 anti-mouse secondary antibody for 1 hour. For BrdU detection, sections were incubated for 30 minutes in 1 M HCl at room temperature, followed by 30 minutes in 2 M HCl at 37°C, then washed in 0.1 M Tris pH 8 and then PBS for 5 minutes, prior to blocking and detection with antibodies as described next for all other antigens. For all other antigens, sections were blocked in 5-10% normal goat serum (Abcam, UK) containing 0.1% Triton (Sigma, UK) for 1 hour, followed by overnight incubation in primary antibody, in dilutions described earlier, and then incubated for 1 hour with an appropriate secondary antibody. Sections were mounted with either VECTASHIELD mounting medium containing DAPI (Vectorlabs Inc.) or treated with 5 µg/ml propidium iodide (Sigma, UK) and 10 µg/ml RNase A (Sigma, UK) for 20 minutes prior to mounting with CITIFLUOR^{TM} (Citifluor Ltd).

For immunocytochemistry on cultured cells, cells were grown on glass coverslips (VWR International, UK), fixed for 15 minutes at room temperature in 4% PFA and further treated as described above.

Imaging and quantification of cell numbers

In vivo comparisons were performed on sagittal midline sections at comparable levels in the same lobules in transgenic and wild-type cerebella. Images of cultured cells and most tissue sections were captured using a Leica DM5000B automated epifluorescence microscope fitted with a Leica DFC425 CCD camera (Leica Microsystems). Single z-planes of sections labelled for BMI1, BrdU and BrdU/EdU were captured with a Zeiss LSM510 confocal microscope with a Meta detector and Argon and He/Ne lasers. For BrdU/EdU images, five to seven z-stacks were acquired at 1.7 µm intervals in lobule VII. For quantification purposes, z-stacks were averaged in ImageJ (NIH, USA) and all double-positive cells in the EGL counted and expressed as an index of positive cells per µm^2. Quantification of total BrdU and the BrdU^{low} indices were performed on images of lobule VII using ImageJ and distinct threshold settings were set to identify positive cells based on

distinct labelling intensities. Quantification of all other immunohistochemistry experiments was performed on single z-planes. Quantification of cell number in the EGL was performed on 63× confocal images, stained with DAPI/EdU/BrdU. The number of cells along the length of the EGL in a perpendicular line from the surface was counted. Four individual lines of cells, representing the longest lines of cells in the EGL, per image were counted to calculate the average length of the EGL in cell number. The IGL cell density was quantified in ImageJ by performing an automatic cell count of propidium-iodide-stained sections with specified parameters for particle size and labelling intensity, and expressed as number of cells per µm^2. Quantification of cell numbers in cultures was performed manually on four representative images/well and at least four wells per genotype per experiment.

Cerebellar weight estimation

Brains (P22, P28) were isolated from wild-type and transgenic littermates and fixed overnight in 4% PFA at 4°C. The cerebellum was dissected away from the rest of the brain, blotted on Whatman filter paper to disregard excess fluid, and weighed on a Sartorius weighing scale.

BrdU and BrdU/EdU administration

For in vivo analysis, BrdU and EdU were administered at 50 mg/kg body weight. For BrdU/EdU double-labelling experiments, P7 pups were injected intraperitoneally with BrdU (Sigma, UK), followed by EdU (Click-iT® EdU kit, Roche, UK) 16.5 hours later. At 30 minutes after the EdU injection, pups were sacrificed and analysed. For BrdU cumulative labelling experiments, BrdU was injected intraperitoneally in P4 pups, followed by a second injection at P5 (24 hours later). Pups were analysed at P6.

For in vitro analysis, to assess cell proliferation over time (DIV1-3), fresh medium containing 10 µM BrdU was added on DIV1 and cultures were stopped at DIV2 and DIV3 and analysed. To assess cell proliferation at a snapshot in time, DIV4 cultures were treated with 10 µM BrdU in fresh medium for 30 minutes and then analysed.

Primary cerebellar cell and DAOY cell line culture

Mixed cerebellar cultures were established from P7-P8 pups as previously described (Subkhankulova et al., 2010). Cells were cultured in the same medium until needed (no medium replacement) in 12-well (1.2×10^6 cells/well) or 24-well (0.6×10^6 cells/well) plates, containing glass coverslips (VWR International, UK), if needed for immunocytochemistry, coated with 100 µg/ml Poly-D-Lysine (Sigma, UK). DAOY cells were cultured in IMEM (Gibco, UK) supplemented with 10% fetal calf serum and 1% penicillin-streptomycin (Invitrogen, UK).

BMI1 knockdown in DAOY cells

DAOY cells seeded at 1×10^4 cells/well in a 24-well plate were allowed to attach for 30 minutes and then HiPerfect transfection reagent (Qiagen, UK) with scrambled siRNA (Qiagen, Cat# 1027280, 30 nM) or BMI1 siRNA [Qiagen, Hs_BMI1_1 (SI03051874), Hs_BMI1_2 (SI03053610), Hs_PCGF4_3 (SI00073325)] was added according to the manufacturer's description. 48 hours later, cells were collected for analysis.

Stress assays

For the hypoxia assay, DIV2 cerebellar cultures were transferred to a 0.2% O_2 humidified hypoxia chamber and incubated at 37°C for 3 hours. The medium was exchanged with fresh medium and cultures were incubated under normoxic conditions for 1-24 hours (5% CO_2, balance O_2 at 37°C).

For the glutamate assay, DIV7 cultures were established as described earlier and treated with either 100 μM glutamate (Sigma, UK) or Locke buffer (control) for 45 minutes at room temperature as described (Ankarcrona et al., 1995) and cultured for another 24 hours in medium without serum under normal conditions (5% CO_2, balance O_2 at 37°C), after which they were analysed.

Measurement of ROS

Transfected DAOY cells (48 hours post transfection) or DIV2 cerebellar mixed cultures (after 3 hours of hypoxia/normoxia treatment) were incubated with 40 μM H_2DCFDA (Invitrogen, UK) in normoxic conditions for 1 hour followed by flow cytometry analysis using an LSRII instrument (Becton-Dickinson) to detect intracellular ROS.

Histology

Brains were fixed in 10% formalin, embedded in paraffin, cut at 5 μm thickness and stained with H&E, all according to standard procedures.

Human medulloblastoma expression profiling and molecular subgrouping

An array-based transcriptome analysis of primary human medulloblastomas (*n*=103) and normal cerebella (fetal, *n*=9; adult, *n*=5) was performed using Affymetrix Genechip Human Exon 1.0ST arrays at The Centre for Applied Genomics (TCAG; www.tcag.ca; Toronto, Canada). Affymetrix Expression Console (Version 1.1) was used to analyse expression data, as previously described (Northcott et al., 2011). Using a gene-expression classifier method, molecular subgroup (WNT, SHH, Group 3, Group 4) was assigned to each tumour, as outlined in Northcott et al. (Northcott et al., 2011).

Statistical analysis

Data were collected from at least three individual wild-type and three transgenic littermates per analysis and 3-11 sections per animal in the vermis of the cerebellum, at equivalent levels, or from four fields of view from three or four coverslips with cultured cells. Data were checked for normality and analysed with either parametric or non-parametric tests accordingly. Gene expression data, cerebellar and body weight data, cell number in EGL, and cell number in cultures were analysed with the independent samples *t*-test. Cell density, BrdU, BrdU/EdU and the GFAP indices, were analysed with ANCOVA with the area or total number of cells used as a covariate. The ROS data in normoxia conditions were analysed with a two-way ANOVA with the effect of genotype and each culture taken into account. The percentage increase in ROS levels upon shifting from normoxia to hypoxia was analysed with a three-way ANOVA, which allowed testing for the effect of oxygenation and genotype on ROS production per preparation. The glutamate assay data were analysed with a three-way ANOVA testing for the effect of genotype, treatment and preparation on cell survival.

REFERENCES

Ajioka, I., Martins, R. A., Bayazitov, I. T., Donovan, S., Johnson, D. A., Frase, S., Cicero, S. A., Boyd, K., Zakharenko, S. S. and Dyer, M. A. (2007). Differentiated horizontal interneurons clonally expand to form metastatic retinoblastoma in mice. *Cell* **131**, 378-390.

Ankarcrona, M., Dypbukt, J. M., Bonfoco, E., Zhivotovsky, B., Orrenius, S., Lipton, S. A. and Nicotera, P. (1995). Glutamate-induced neuronal death: a succession of necrosis or apoptosis depending on mitochondrial function. *Neuron* **15**, 961-973.

Bahn, S., Jones, A. and Wisden, W. (1997). Directing gene expression to cerebellar granule cells using gamma-aminobutyric acid type A receptor alpha6 subunit transgenes. *Proc. Natl. Acad. Sci. USA* **94**, 9417-9421.

Behesti, H. and Marino, S. (2009). Cerebellar granule cells: insights into proliferation, differentiation, and role in medulloblastoma pathogenesis. *Int. J. Biochem. Cell Biol.* **41**, 435-445.

Chatoo, W., Abdouh, M., David, J., Champagne, M. P., Ferreira, J., Rodier, F. and Bernier, G. (2009). The polycomb group gene Bmi1 regulates antioxidant defenses in neurons by repressing p53 pro-oxidant activity. *J. Neurosci.* **29**, 529-542.

Chen, G., Ma, C., Bower, K. A., Shi, X., Ke, Z. and Luo, J. (2008). Ethanol promotes endoplasmic reticulum stress-induced neuronal death: involvement of oxidative stress. *J. Neurosci. Res.* **86**, 937-946.

Chen, Y. and Swanson, R. A. (2003). Astrocytes and brain injury. *J. Cereb. Blood Flow Metab.* **23**, 137-149.

Dai, Y. and Grant, S. (2003). New insights into checkpoint kinase 1 in the DNA damage response signaling network. *Clin. Cancer Res.* **16**, 376-383.

Davies, N. P., Wilson, M., Harris, L. M., Natarajan, K., Lateef, S., Macpherson, L., Sgouros, S., Grundy, R. G., Arvanitis, T. N. and Peet, A. C. (2008). Identification and characterisation of childhood cerebellar tumours by in vivo proton MRS. *NMR Biomed.* **21**, 908-918.

Dobles, M., Liberal, V., Scott, M. L., Benezra, R. and Sorger, P. K. (2000). Chromosome missegregation and apoptosis in mice lacking the mitotic checkpoint protein Mad2. *Cell* **101**, 635-645.

Donehower, L. A., Harvey, M., Slagle, B. L., McArthur, M. J., Montgomery, C. A., Jr, Butel, J. S. and Bradley, A. (1992). Mice deficient for p53 are developmentally normal but susceptible to spontaneous tumours. *Nature* **356**, 215-221.

Ellison, D. (2002). Classifying the medulloblastoma: insights from morphology and molecular genetics. *Neuropathol. Appl. Neurobiol.* **28**, 257-282.

Facchino, S., Abdouh, M., Chatoo, W. and Bernier, G. (2010). BMI1 confers radioresistance to normal and cancerous neural stem cells through recruitment of the DNA damage response machinery. *J. Neurosci.* **30**, 10096-10111.

Fasano, C. A., Dimos, J. T., Ivanova, N. B., Lowry, N., Lemischka, I. R. and Temple, S. (2007). shRNA knockdown of Bmi1 reveals a critical role for p21-Rb pathway in NSC self-renewal during development. *Cell Stem Cell* **1**, 87-99.

Fasano, C. A., Phoenix, T. N., Kokovay, E., Lowry, N., Elkabetz, Y., Dimos, J. T., Lemischka, I. R., Studer, L. and Temple, S. (2009). Bmi-1 cooperates with Foxg1 to maintain neural stem cell self-renewal in the forebrain. *Genes Dev.* **23**, 561-574.

Frandsen, A. and Schousboe, A. (1990). Development of excitatory amino acid induced cytotoxicity in cultured neurons. *Int. J. Dev. Neurosci.* **8**, 209-216.

Fujita, S. (1967). Quantitative analysis of cell proliferation and differentiation in the cortex of the postnatal mouse cerebellum. *J. Cell Biol.* **32**, 277-287.

Fujita, S., Shimada, M. and Nakamura, T. (1966). H3-thymidine autoradiographic studies on the cell proliferation and differentiation in the external and the internal granular layers of the mouse cerebellum. *J. Comp. Neurol.* **128**, 191-208.

Goodrich, L. V., Milenkovic, L., Higgins, K. M. and Scott, M. P. (1997). Altered neural cell fates and medulloblastoma in mouse patched mutants. *Science* **277**, 1109-1113.

Halfter, H., Friedrich, M., Resch, A., Kullmann, M., Stogbauer, F., Ringelstein, E. B. and Hengst, L. (2006). Oncostatin M induces growth arrest by inhibition of Skp2, Cks1, and cyclin A expression and induced p21 expression. *Cancer Res.* **66**, 6530-6539.

Harvey, M., McArthur, M. J., Montgomery, C. A., Jr, Butel, J. S., Bradley, A. and Donehower, L. A. (1993). Spontaneous and carcinogen-induced tumorigenesis in p53-deficient mice. *Nat. Genet.* **5**, 225-229.

Haupt, Y., Bath, M. L., Harris, A. W. and Adams, J. M. (1993). bmi-1 transgene induces lymphomas and collaborates with myc in tumorigenesis. *Oncogene* **8**, 3161-3164.

He, S., Iwashita, T., Buchstaller, J., Molofsky, A. V., Thomas, D. and Morrison, S. J. (2009). Bmi-1 over-expression in neural stem/progenitor cells increases proliferation and neurogenesis in culture but has little effect on these functions in vivo. *Dev. Biol.* **328**, 257-272.

Jackson, S. P. and Bartek, J. (2009). The DNA-damage response in human biology and disease. *Nature* **461**, 1071-1078.

Kato, K. (1990). Novel GABAA receptor alpha subunit is expressed only in cerebellar granule cells. *J. Mol. Biol.* **214**, 619-624.

Kessler, J. D., Hasegawa, H., Brun, S. N., Emmenegger, B. A., Yang, Z. J., Dutton, J. W., Wang, F. and Wechsler-Reya, R. J. (2009). N-myc alters the fate of preneoplastic cells in a mouse model of medulloblastoma. *Genes Dev.* **23**, 157-170.

Kool, M., Koster, J., Bunt, J., Hasselt, N. E., Lakeman, A., van Sluis, P., Troost, D., Meeteren, N. S., Caron, H. N., Cloos, J. et al. (2008). Integrated genomics identifies five medulloblastoma subtypes with distinct genetic profiles, pathway signatures and clinicopathological features. *PLoS ONE* **3**, e3088.

Leung, C., Lingbeek, M., Shakhova, O., Liu, J., Tanger, E., Saremaslani, P., Van Lohuizen, M. and Marino, S. (2004). Bmi1 is essential for cerebellar development and is overexpressed in human medulloblastomas. *Nature* **428**, 337-341.

Liu, J., Cao, L., Chen, J., Song, S., Lee, I. H., Quijano, C., Liu, H., Keyvanfar, K., Chen, H., Cao, L. Y. et al. (2009). Bmi1 regulates mitochondrial function and the DNA damage response pathway. *Nature* **459**, 387-392.

Lumpkin, E. A., Collisson, T., Parab, P., Omer-Abdalla, A., Haeberle, H., Chen, P., Doetzlhofer, A., White, P., Groves, A., Segil, N. et al. (2003). Math1-driven GFP expression in the developing nervous system of transgenic mice. *Gene. Expr. Patterns* **3**, 389-395.

Machold, R. and Fishell, G. (2005). Math1 is expressed in temporally discrete pools of cerebellar rhombic-lip neural progenitors. *Neuron* **48**, 17-24.

Marino, S., Vooijs, M., van der Gulden, H., Jonkers, J. and Berns, A. (2000). Induction of medulloblastomas in p53-null mutant mice by somatic inactivation of Rb in the external granular layer cells of the cerebellum. *Genes Dev.* **14**, 994-1004.

Molofsky, A. V., Pardal, R., Iwashita, T., Park, I. K., Clarke, M. F. and Morrison, S. J. (2003). Bmi-1 dependence distinguishes neural stem cell self-renewal from progenitor proliferation. *Nature* **425**, 962-967.

Molofsky, A. V., He, S., Bydon, M., Morrison, S. J. and Pardal, R. (2005). Bmi-1 promotes neural stem cell self-renewal and neural development but not mouse growth and survival by repressing the p16Ink4a and p19Arf senescence pathways. *Genes Dev.* **19**, 1432-1437.

Mullen, R. J., Buck, C. R. and Smith, A. M. (1992). NeuN, a neuronal specific nuclear protein in vertebrates. *Development* **116**, 201-211.

Northcott, P. A., Korshunov, A., Witt, H., Hielscher, T., Eberhart, C. G., Mack, S., Bouffet, E., Clifford, S. C., Hawkins, C. E., French, P. et al. (2011). Medulloblastoma comprises four distinct molecular variants. *J. Clin. Oncol.* **29**, 1408-1414.

Pomeroy, S. L., Tamayo, P., Gaasenbeek, M., Sturla, L. M., Angelo, M., McLaughlin, M. E., Kim, J. Y., Goumnerova, L. C., Black, P. M., Lau, C. et al. (2002). Prediction of central nervous system embryonal tumour outcome based on gene expression. *Nature* **415**, 436-442.

Sancar, A., Lindsey-Boltz, L. A., Unsal-Kacmaz, K. and Linn, S. (2004). Molecular mechanisms of mammalian DNA repair and the DNA damage checkpoints. *Annu. Rev. Biochem.* **73**, 39-85.

Sasaki, T., Ito, Y., Xu, X., Han, J., Bringas, P., Jr, Maeda, T., Slavkin, H. C., Grosschedl, R. and Chai, Y. (2005). LEF1 is a critical epithelial survival factor during tooth morphogenesis. *Dev. Biol.* **278**, 130-143.

Schafer, Z. T., Grassian, A. R., Song, L., Jiang, Z., Gerhart-Hines, Z., Irie, H. Y., Gao, S., Puigserver, P. and Brugge, J. S. (2009). Antioxidant and oncogene rescue of metabolic defects caused by loss of matrix attachment. *Nature* **461**, 109-113.

Schuller, U., Heine, V. M., Mao, J., Kho, A. T., Dillon, A. K., Han, Y. G., Huillard, E., Sun, T., Ligon, A. H., Qian, Y. et al. (2008). Acquisition of granule neuron precursor identity is a critical determinant of progenitor cell competence to form Shh-induced medulloblastoma. *Cancer Cell* **14**, 123-134.

Skokowa, J., Cario, G., Uenalan, M., Schambach, A., Germeshausen, M., Battmer, K., Zeidler, C., Lehmann, U., Eder, M., Baum, C. et al. (2006). LEF-1 is crucial for neutrophil granulocytopoiesis and its expression is severely reduced in congenital neutropenia. *Nat. Med.* **12**, 1191-1197.

Spaulding, C., Reschly, E. J., Zagort, D. E., Yashiro-Ohtani, Y., Beverly, L. J., Capobianco, A., Pear, W. S. and Kee, B. L. (2007). Notch1 co-opts lymphoid enhancer factor 1 for survival of murine T-cell lymphomas. *Blood* **110**, 2650-2658.

Subkhankulova, T., Zhang, X., Leung, C. and Marino, S. (2010). Bmi1 directly represses p21Waf1/Cip1 in Shh-induced proliferation of cerebellar granule cell progenitors. *Mol. Cell Neurosci.* **45**, 151-162.

Taylor, M. D., Northcott, P. A., Korshunov, A., Remke, M., Cho, Y. J., Clifford, S. C., Eberhart, C. G., Parsons, D. W., Rutkowski, S., Gajjar, A. et al. (2012). Molecular subgroups of medulloblastoma: the current consensus. *Acta Neuropathol.* **123**, 465-472.

Thompson, M. C., Fuller, C., Hogg, T. L., Dalton, J., Finkelstein, D., Lau, C. C., Chintagumpala, M., Adesina, A., Ashley, D. M., Kellie, S. J. et al. (2006). Genomics identifies medulloblastoma subgroups that are enriched for specific genetic alterations. *J. Clin. Oncol.* **24**, 1924-1931.

Valk-Lingbeek, M. E., Bruggeman, S. W. and van Lohuizen, M. (2004). Stem cells and cancer; the polycomb connection. *Cell* **118**, 409-418.

van der Lugt, N. M., Domen, J., Linders, K., van Roon, M., Robanus-Maandag, E., te Riele, H., van der Valk, M., Deschamps, J., Sofroniew, M., van Lohuizen, M. et al. (1994). Posterior transformation, neurological abnormalities, and severe hematopoietic defects in mice with a targeted deletion of the bmi-1 proto-oncogene. *Genes Dev.* **8**, 757-769.

Wingate, R. J. and Hatten, M. E. (1999). The role of the rhombic lip in avian cerebellum development. *Development* **126**, 4395-4404.

Wu, V. W. and Schwartz, J. P. (1998). Cell culture models for reactive gliosis: new perspectives. *J. Neurosci. Res.* **51**, 675-681.

Yadirgi, G., Leinster, V. H., Acquati, S., Bhagat, H., Shakhova, O. and Marino, S. (2011). Conditional activation of Bmi1 expression regulates self renewal, apoptosis and differentiation of neural stem/progenitor cells in vitro and in vivo. *Stem Cells* **29**, 700-712.

Yang, Z. J., Ellis, T., Markant, S. L., Read, T. A., Kessler, J. D., Bourboulas, M., Schuller, U., Machold, R., Fishell, G., Rowitch, D. H. et al. (2008). Medulloblastoma can be initiated by deletion of Patched in lineage-restricted progenitors or stem cells. *Cancer Cell* **14**, 135-145.

Yoshioka, A., Ikegaki, N., Williams, M. and Pleasure, D. (1996). Expression of N-methyl-D-aspartate (NMDA) and non-NMDA glutamate receptor genes in neuroblastoma, medulloblastoma, and other cells lines. *J. Neurosci. Res.* **46**, 164-178.

Yoshioka, H., Mino, M., Morikawa, Y., Kasubuchi, Y. and Kusunoki, T. (1985). Changes in cell proliferation kinetics in the mouse cerebellum after total asphyxia. *Pediatrics* **76**, 965-969.

Zinkel, S., Gross, A. and Yang, E. (2006). BCL2 family in DNA damage and cell cycle control. *Cell Death Differ.* **13**, 1351-1359.
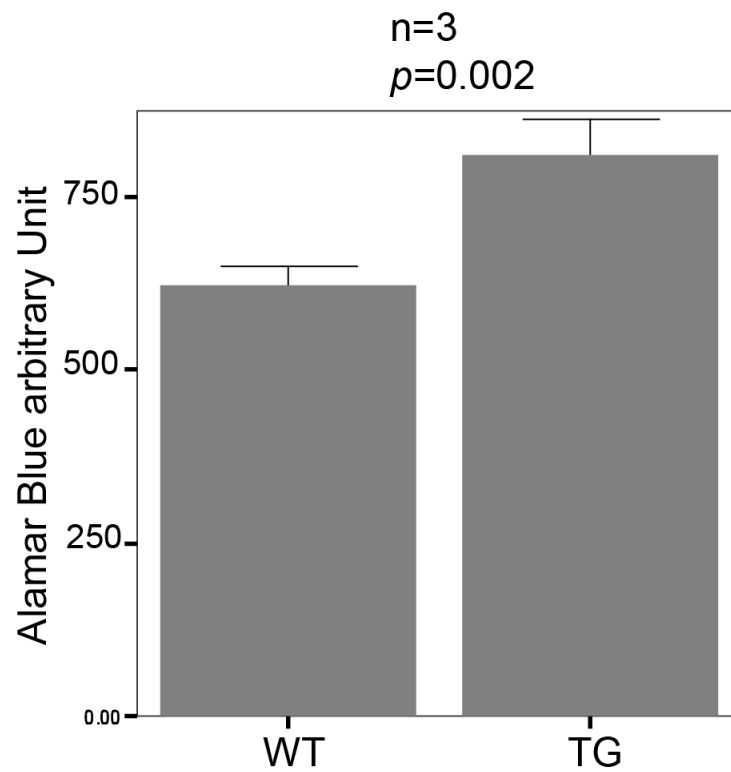
Fig. S1. Alamar blue assay at DIV7 in *Gabra6-Bmi1* and wild-type cultures. Arbitrary colourimetric units of Alamar blue measured by a plate reader according to the manufacturer's description (Biosource International Inc., USA) at DIV7 in wild-type (WT) and transgenic (TG) cultures showing lower survival/metabolism in wild-type cultures. Bars show mean +/− 1 s.e.m. P-value by independent sample's *t*-test.